Minimal Model for Carnot Efficiency at Maximum Power

Shiling Liang (梁师翎),[1,2,*] Yu-Han Ma,[3,4,†] Daniel Maria Busiello,[5,7] and Paolo De Los Rios[1,6]
[1]Institute of Physics, School of Basic Sciences, École Polytechnique Fédérale de Lausanne (EPFL), 1015 Lausanne, Switzerland
[2]Biological Complexity Unit, Okinawa Institute of Science and Technology Graduate University, Onna, Okinawa 904-0495, Japan
[3]School of Physics and Astronomy, Beijing Normal University, Beijing, 100875, China
[4]Graduate School of China Academy of Engineering Physics, Beijing, 100193, China
[5]Max Planck Institute for the Physics of Complex Systems, 01187 Dresden, Germany
[6]Institute of Bioengineering, School of Life Sciences, École Polytechnique Fédérale de Lausanne (EPFL), 1015 Lausanne, Switzerland
[7]Department of Physics and Astronomy "G. Galilei," University of Padova, 35131 Padova, Italy

(Received 14 December 2023; revised 9 July 2024; accepted 10 December 2024; published 13 January 2025)

Carnot efficiency sets a fundamental upper bound on the heat engine efficiency, attainable in the quasistatic limit, albeit at the cost of completely sacrificing power output. Here, we present a minimal heat engine model that can attain Carnot efficiency while achieving maximum power output. We unveil the potential of intrinsic divergent physical quantities within the working substance, such as degeneracy, as promising thermodynamic resources to break through the universal power-efficiency trade-off imposed by nonequilibrium thermodynamics for conventional heat engines. Our findings provide novel insights into the collective advantage in harnessing energy of many-body interacting systems.

DOI: 10.1103/PhysRevLett.134.027101

Heat engines generally operate between two thermal baths at different temperatures ($T_h > T_c$), converting thermal energy into output work. Their efficiency, $\eta = W/Q_h$, i.e., the ratio of output work W to absorbed heat Q_h, is bounded by the second law of thermodynamics, with an upper limit defined by the Carnot efficiency $\eta_C = 1 - T_c/T_h$ [1]. Since any finite-time operation in a thermodynamic system leads to irreversible entropy production, the Carnot limit can only be achieved when an engine operates in a quasistatic regime, resulting in zero power output [2,3]. However, functional heat engines require both high efficiency and high output power. To evaluate their performance, efficiency at maximum power (EMP) [4–9] and the trade-off relation between power and efficiency [10–14] have been proposed as key benchmarks, drawing significant attention in nonequilibrium and engineering thermodynamics [15–17].

Recent developments in stochastic thermodynamics paved new ways to investigate heat engines operating far from equilibrium [18]. These developments offer the potential to achieve Carnot efficiency with finite [19–22] or maximum [23,24] power using working substances with intrinsic divergent physical quantities. Many-body interacting systems exploit these properties through emerging collective effects, significantly reducing the irreversible dissipation relative to output work and thus enhancing engine efficiency [22,25–28]. Despite significant progress, a comprehensive understanding of the key advantages stemming from collective operations remains elusive. Key open questions include the existence of a universal power-efficiency trade-off for collective heat engines, and the relationship between engine performance and many-body phase transitions.

To address these problems, we present a minimal model [Fig. 1(a)] that incorporates intrinsic energy level degeneracy, thereby circumventing the complexity while capturing the basic degenerate characteristics arising from many-body interactions. This particular engine can achieve Carnot efficiency at maximum power [Fig. 1(b)]. More importantly, we analytically derive the asymptotic behavior of the power-efficiency trade-off [Fig. 2(f)] in the limit of large degeneracy of the high-energy state. Our findings

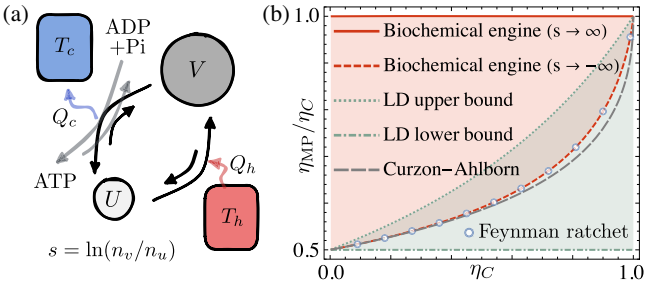


FIG. 1. (a) A biochemical engine operating between two thermal baths to convert thermal into chemical energy through ATP synthesis. U and V are two coarse-grained states with degeneracies n_u and n_v, resulting in an entropy difference $s = \ln(n_v/n_u)$. (b) The EMP of this engine can surpass the universal upper bound for low-dissipation (LD) engines [9] and reach Carnot efficiency at $s \to \infty$.

*Contact author: shiling.liang@epfl.ch
†Contact author: yhma@bnu.edu.cn

 © 2025 American Physical Society

explicitly demonstrate the violation of the $1/2$ universality of EMP [6,29] in the thermodynamic limit (Fig. 3). We show that the thermodynamic advantage of the proposed engine stems from the first-order phase transition occurring far from the linear response regime.

Model—Mesoscopic heat engines can produce work by synthesizing adenosine triphosphate (ATP) [23,30]. In this Letter, we consider a biochemical engine composed of a low-energy state U and a high-energy state V representing two coarse-grained states with n_u and n_v microscopic conformations, respectively [Fig. 1(a)]. For example, U and V can represent the folded and unfolded states of a polymer [31,32] or chemical species [33]. The entropy difference between these two coarse-grained states, $s = \ln(n_v/n_u)$, comes from the degeneracy difference. There are two reaction paths between U and V: an ATP-hydrolysis-driven reaction under low temperature T_c and a spontaneous transition coupled to the high-temperature reservoir T_h:

$$U \underset{k_{h-}}{\overset{k_{h+}}{\rightleftharpoons}} V, \qquad \mathrm{ATP} + U \underset{k^0_{c-}}{\overset{k^0_{c+}}{\rightleftharpoons}} V + \mathrm{ADP} + \mathrm{Pi}.$$

Here $\{k^0_{c+}, k^0_{c-}\}$ denote the forward and backward ATP-driven reaction rates, and $\{k_{h+}, k_{h-}\}$ are the high-temperature spontaneous transition rates. Absorbing the chemostatted concentrations of ATP, adenosine diphosphate (ADP), and phosphate (Pi) into the rates, we can define effective rates $k_{c+} = k^0_{c+}[\mathrm{ATP}]$ and $k_{c-} = k^0_{c-}[\mathrm{ADP}][\mathrm{Pi}]$. All rates must satisfy local detailed balance, $k_{h-}/k_{h+} = e^{\beta_h \epsilon_h - s}$ and $k_{c-}/k_{c+} = e^{\beta_c \epsilon_c - s}$, where $\beta_{h/c} = 1/k_B T_{h/c}$ [34,35]. Here, ϵ_h and ϵ_c are the energy gaps of the system when coupled to the hot and cold reservoirs, respectively. The change of energy gap $\Delta\mu \equiv \epsilon_h - \epsilon_c$ is the output work per cycle in terms of ATP synthesis.

The dynamics of the system is described by the master equation,

$$\begin{aligned} \frac{d}{dt} p_u &= (k_{h-} + k_{c-}) p_v - (k_{h+} + k_{c+}) p_u, \\ \frac{d}{dt} p_v &= (k_{h+} + k_{c+}) p_u - (k_{h-} + k_{c-}) p_v, \end{aligned} \tag{1}$$

where p_u and p_v are the probabilities of two states. Each reaction path has a corresponding equilibrium distribution,

$$\pi_v^{h/c} = \frac{1}{1 + e^{\beta_{h/c}\epsilon_{h/c} - s}}, \qquad \pi_u^{h/c} = \frac{e^{\beta_{h/c}\epsilon_{h/c} - s}}{1 + e^{\beta_{h/c}\epsilon_{h/c} - s}}, \tag{2}$$

that satisfies $\pi_u^h/\pi_v^h = k_{h-}/k_{h+}$ and $\pi_u^c/\pi_v^c = k_{c-}/k_{c+}$.

At stationarity, $p^{\mathrm{ss}}_{u/v} = (\tau_h \pi^c_{u/v} + \tau_c \pi^h_{u/v})/(\tau_h + \tau_c)$ as a consequence of the competition between two reaction paths with typical timescales $\tau_h = (k_{h+} + k_{h-})^{-1}$ and $\tau_c = (k_{c+} + k_{c-})^{-1}$. The corresponding steady-state cyclic current is [36]

$$J^{\mathrm{ss}} = \tau^{-1}(\pi_v^h - \pi_v^c), \tag{3}$$

where $\tau = \tau_h + \tau_c$ is the characteristic time of completing the cycle. The change of internal entropy does not lead to entropy production into the environment [35,37,38], and thus the heat absorption rate from the hot (cold) reservoir is given by $\dot{Q}_h = J^{\mathrm{ss}}\epsilon_h$ ($\dot{Q}_c = -J^{\mathrm{ss}}\epsilon_c$). The steady-state output power is

$$P = J^{\mathrm{ss}}(\epsilon_h - \epsilon_c) = \tau^{-1}(\pi_v^h - \pi_v^c)(\epsilon_h - \epsilon_c), \tag{4}$$

then the thermodynamic efficiency reads

$$\eta = P/\dot{Q}_h = 1 - (\epsilon_c/\epsilon_h). \tag{5}$$

One can find that the quasistatic limit, i.e., $J^{\mathrm{ss}} = 0$, is reached when $\epsilon_c T_h = \epsilon_h T_c$ and leads to Carnot efficiency.

Optimization—To maximize the power of the biochemical engine, we set the entropy difference s as a control parameter and optimize the two energy levels ϵ_c and ϵ_h under different T_h and T_c. For convenience, we set the Boltzmann constant $k_B = 1$, and use $k_B T_h = 1$ as the reference energy. We follow the convention to assume the characteristic time τ constant because it is a kinetic parameter and thus not constrained by thermodynamics in general cases [8]. Therefore, we optimize the work of the thermodynamic cycle,

$$W = \tau P = (\pi_v^h - \pi_v^c)(\epsilon_h - \epsilon_c) \equiv W_{\mathrm{Otto}}, \tag{6}$$

which has an intuitive geometric representation in the state space, as shown in Fig. 2(a). Indeed, it corresponds to the work of an Otto cycle $abcda$ operating between two thermal reservoirs (see [36] for a detailed comparison). Hereafter, we rescale physical quantities by s such that $\bar{x} \equiv x/s$, since s characterizes the system size, as discussed below. In the Otto cycle, the two quench processes $d \to a$ and $b \to c$ do not have intrinsic speed limits while the two isothermal relaxations $c \to d$ and $a \to b$ have intrinsic relaxation timescales $\tau_{h/c} = k_{h/c}^{-1}$ that set $\tau = \tau_h + \tau_c$ as the time of completing the cycle [36].

Let us start with limiting cases. In Fig. 1(b), we present EMP, η_{MP}, as a function of η_C. When $s \to -\infty$, we can expand p_u^{ss} with respect to e^s, so that the power becomes $P = [T_c e^s (e^{-\theta(1-\eta)} - e^{-\theta(1-\eta_C)})\eta\theta]/\tau$, where $\theta \equiv \epsilon_h \beta_c$. This expression has the same mathematical structure as Feynman's ratchet heat engine whose closed-form EMP has been obtained in [8]. The resulting EMP [blue dots in Fig. 1(b)] serves as the lower bound for the biochemical engine and is higher than the Curzon-Ahlborn efficiency [5].

For large s, i.e., high degeneracy of the high-energy state, a closed-form EMP cannot be obtained. However, numerical optimization of Eq. (4) [39] shows that η_{MP}

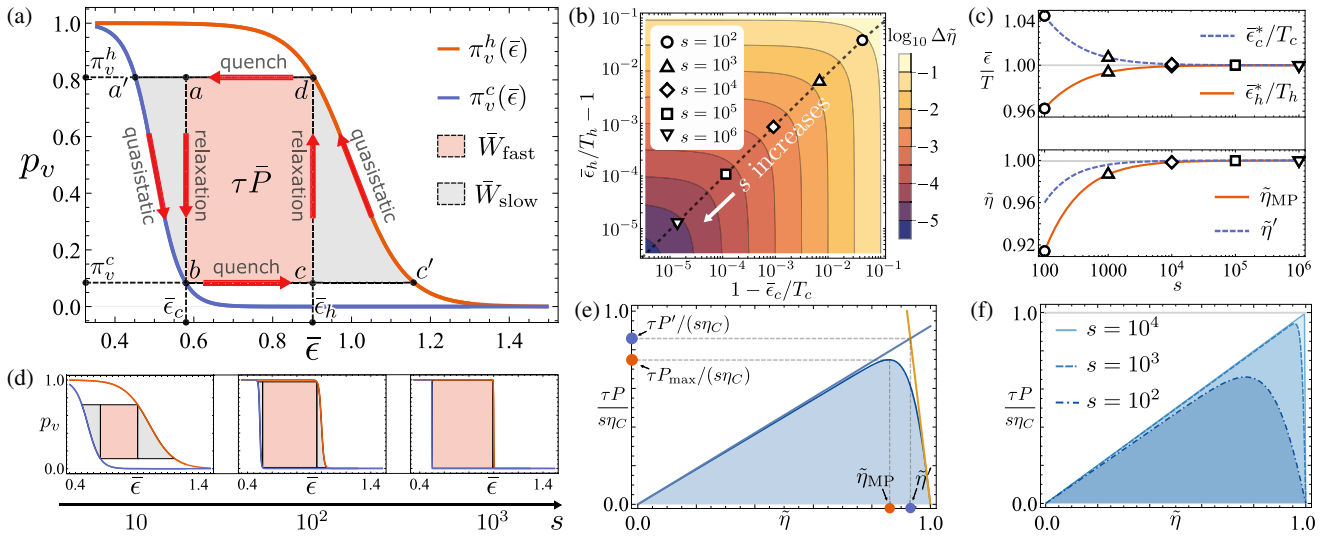


FIG. 2. Optimization of the biochemical engine. (a) An Otto cycle, $abcda$, operates between two thermal reservoirs. Red and blue curves denote the equilibrium population on state v coupled to T_h and T_c, respectively. $a'bc'da'$ is a Carnot cycle. (b) Deviation from Carnot efficiency $\Delta\tilde{\eta} = 1 - \eta/\eta_C$ as a function of thermodynamic parameters $\bar{\epsilon}_h/T_h$ and $\bar{\epsilon}_c/T_c$. Points and dashed line indicate optimal parameters, $\bar{\epsilon}_h^*$ and $\bar{\epsilon}_c^*$, that maximize the power for different s. (c) In the large-s limit, maximum power is reached when $\bar{\epsilon}_{c/h}^*/T_{c/h} \to 1$, while the rescaled EMP approaches the Carnot limit, $\tilde{\eta}_{\rm MP} \equiv \eta_{\rm MP}/\eta_C \to 1$. (d) Optimized Otto cycles to attain maximum output work under different values of s. (e) Power-efficiency trade-off and linear expansion lines from the two end points $\tilde{\eta} \to 0$ and $\tilde{\eta} \to 1$. The intersection of these lines gives upper bounds on maximum power P' and corresponding efficiency η'. (f) Power-efficiency trade-off at different s, obtained via numerical optimization [39], reveals power scaling with $s\eta_C$ at large s. We set $k_B T_h = 1$ as the reference energy and $\eta_C = 0.5$.

surpasses the universal upper bound $\eta_C/(2-\eta_C)$ of low-dissipation heat engines [9] and approaches the Carnot efficiency as $s \to \infty$ [Fig. 1(b), red solid line]. In Fig. 2(b), we illustrate the efficiency of the biochemical engine as a function of the thermodynamic parameters $\bar{\epsilon}_h/T_h$ and $\bar{\epsilon}_c/T_c$. The color map represents the relative deviation of efficiency from η_C, $\Delta\tilde{\eta} \equiv 1 - \eta/\eta_C$, which approaches 0 in the $s \to \infty$ limit. Markers and dashed line indicate $(\bar{\epsilon}_h^*, \bar{\epsilon}_c^*)$ that maximize the power at different s. Figures 2(b) and 2(c) together indicate that the optimizations of power and efficiency coincide in the large-s limit and lead to Carnot efficiency at maximum power.

Thermodynamic advantage of phase transition—As illustrated in Fig. 2(c), in the large-s limit, the maximum power is achieved when $\bar{\epsilon}_{h/c}^*/T_{h/c} \to 1$. These optimized energy gaps correspond to the most sensitive region of the equilibrium curves $\pi_v^{h/c}(\bar{\epsilon})$, as shown in Fig. 2(d). Since the slope,

$$\left.\frac{\mathrm{d}\pi_v^{h/c}(\bar{\epsilon})}{\mathrm{d}\bar{\epsilon}}\right|_{\bar{\epsilon}=T_{h/c}} = -\frac{s}{4T_{h/c}}, \tag{7}$$

scales linearly with s, when $s \to \infty$, $T_{h/c} = \bar{\epsilon}_{h/c}$ are two phase-transition points with diverging slope. At infinite s, when $\bar{\epsilon}_h$ crosses this point, the equilibrium distribution π_v^h transitions from 0 to 1 [Fig. 2(d), red line], and the same holds for π_v^c [Fig. 2(d), blue line], consequently inducing an abrupt change in p_v during relaxation.

To understand the physical meaning of the $s \to \infty$ limit, we consider the simple example of N interacting units that can be in an inactive ($\sigma_i = 0$) or active ($\sigma_i = 1$) state and exhibit N-body interactions with the Hamiltonian $H = -\epsilon \prod_{i=1}^N \sigma_i$. This system has two coarse-grained states: a low-energy one U, with $E_U = -\epsilon$ where all units are active, and a high-energy state V, with $E_V = 0$ with at least one inactive unit. Their degeneracies are $n_u = 1$ and $n_v = 2^N - 1$, respectively. Their entropy difference $s = \ln(n_v/n_u) \simeq N \ln 2$ for large N, thus scaling linearly with N and diverging at the thermodynamic limit $N \to \infty$. By coupling this system to two reservoirs, we recover our minimal model. While this N-body interaction is idealized, it captures the essential physics. Importantly, recent studies show that properly designed two-body interacting systems can exhibit similar collective advantage [25,40], suggesting a broad applicability for our findings.

A geometrical analysis of thermodynamic cycles at increasing s will clarify the role of the phase transition in enhancing engine performance. In the Otto cycle, irreversible dissipation originates from two relaxation processes and is quantified by the Kullback-Leibler divergence between their corresponding initial and final states [41,42]. To prevent irreversible dissipation, the Carnot cycle $a'bc'da'$ should be employed. It includes two quasistatic processes whose associated work is denoted

by W_{slow} [Fig. 2(a), where $\bar{W}_{\mathrm{slow/fast}}$ represents the work rescaled by s]. The quality of the Otto cycle can be assessed by defining the quality factor $\mathcal{Q}$ as the ratio of its work, $W_{\mathrm{Otto}} \equiv W_{\mathrm{fast}}$ to the work of the Carnot cycle, $W_{\mathrm{Carnot}} \equiv W_{\mathrm{fast}} + W_{\mathrm{slow}}$. When $s \gg 1$, we find [36]

$$\mathcal{Q} \equiv \frac{W_{\mathrm{Otto}}}{W_{\mathrm{Carnot}}} = \frac{W_{\mathrm{fast}}}{W_{\mathrm{fast}} + W_{\mathrm{slow}}} \simeq \left.\frac{\bar{\epsilon}_h - \bar{\epsilon}_c}{T_h - T_c}\right|_{s\gg 1}. \tag{8}$$

Thus, the power-optimized biochemical engine operates close to the phase transition points in both reservoirs, i.e., $T_{h/c}/\bar{\epsilon}^*_{h/c} \to 1$, $\mathcal{Q}$ approaches 1, and the Otto cycle coincides with the Carnot cycle [Fig. 2(d)].

We conclude that the first-order phase transition induced by the divergence of high-energy level degeneracy is a favorable thermodynamic resource, allowing the EMP to approach Carnot efficiency. Previous studies reporting thermodynamic advantages stemming from phase transitions were limited to finite power [22], quasistatic cycles [43], and slow-driving regimes [21]. We emphasize that our model not only pinpoints the minimal ingredients that capture the thermodynamic advantage of phase transition but also suggests that this advantage persists even in fast-driving scenarios, where the protocol involves effective quenching processes which are infinitely faster than the intrinsic engine timescale.

Power-efficiency trade-off—Substituting Eqs. (2) and (5) into Eq. (4), the power can be written in terms of ϵ_h and the rescaled efficiency $\tilde{\eta} \equiv \eta/\eta_C$ as

$$P = \tilde{\eta}\epsilon_h \tau^{-1}\left(\frac{\eta_C}{e^{\epsilon_h - s}+1} - \frac{\eta_C}{e^{\frac{\epsilon_h(1-\tilde{\eta}\eta_C)}{1-\eta_C} - s}+1}\right). \tag{9}$$

The power-efficiency trade-off curve is obtained by numerically maximizing P with respect to ϵ_h [39], i.e., $\partial_{\epsilon_h} P(\epsilon_h, \tilde{\eta}; \eta_C, s) = 0$ [11–13,44] [Figs. 2(e) and 2(f)]. By expanding around the ends $\tilde{\eta} \approx 0$ and $\tilde{\eta} \approx 1$ for large s [Fig. 2(e)] [36], we obtain the following limiting behaviors for the power-efficiency trade-off:

$$\begin{aligned} &\lim_{\tilde{\eta}\to 0} P \simeq \tau^{-1}(s - \ln s)\eta_C \tilde{\eta}, \\ &\lim_{\tilde{\eta}\to 1} P \simeq \frac{\tau^{-1} s^2 \eta_C^2}{4(1-\eta_C)}(1-\tilde{\eta}). \end{aligned} \tag{10}$$

As shown in Fig. 2(f), when $s \to \infty$, the shape of the trade-off curve approaches an isosceles right triangle in the rescaled parametric space, showing that maximum power and Carnot efficiency are achieved simultaneously.

To elucidate this behavior, we approximate the maximum power and EMP with the intersection points of the two expansions in Eq. (10), named P' and $\tilde{\eta}'$, respectively, and illustrated in Fig. 2(e):

$$P_{\max} \simeq P' \simeq s\eta_C/\tau, \qquad \tilde{\eta}_{\mathrm{MP}} \simeq \tilde{\eta}' \simeq 1 - \frac{4(1-\eta_C)}{s\eta_C}. \tag{11}$$

The difference between $\tilde{\eta}_{\mathrm{MP}}$ and $\tilde{\eta}'$ decreases as s increases, and they both converge toward the Carnot efficiency ($\tilde{\eta} = 1$) for $s \to \infty$. We note that the EMP in Eq. (11) recovers the result of [24] where the authors found the EMP by solving for the global maximum power. The power-efficiency trade-off presented in the current work provides complete performance information, such as the maximum efficiency at arbitrary power and the maximum power at arbitrary efficiency, for heat engines whose working substances exhibit degeneracy.

Equation (11) indicates that the maximum power scales as $s\eta_C$ while the corresponding EMP approaches Carnot efficiency as $(s\eta_C)^{-1}$ [Figs. 2(c) and 2(f)]. This scaling relation can be seen as $\lim_{s\gg 1} P_{\max} \simeq s k_B \Delta T/\tau$, where $\Delta T \equiv T_h - T_c$. For the example of interacting unit σ_i, discussed before, $s \propto N$ in the large-s regime; thus the power of each unit satisfies $P_I = P/N \sim k_B \Delta T/\tau$.

In a recent study [44], Shiraishi *et al.* proposed a universal power-efficiency trade-off as

$$P \le \Theta \beta_c \eta_C^2 \tilde{\eta}(1-\tilde{\eta}), \tag{12}$$

where Θ relates to state and size of the heat engine. For finite-size heat engines, Θ remains finite; thus Carnot efficiency cannot be reached with finite power. However, with divergent system size, Θ may also diverge, allowing the Carnot efficiency to be approached arbitrarily closely even at maximum power, as for quantum heat engines with coherence [28]. In this respect, we show that also our classic engine benefits from the scaling relationships with system size. Comparing Eq. (12) with Eq. (10), we obtain the prefactor Θ as

$$\begin{cases} \Theta_0 \equiv \lim_{\tilde{\eta}\to 0}\Theta \simeq \frac{(s-\ln s)}{\tau\eta_C\beta_c} \\ \Theta_1 \equiv \lim_{\tilde{\eta}\to 1}\Theta \simeq \frac{\tau^{-1}s^2}{4(1-\eta_C)\beta_c} \end{cases} \Rightarrow \frac{\Theta_1}{\Theta_0} \sim s, \tag{13}$$

with the ratio of the two prefactors scaling linearly with s in the large-s limit. Note that, although we have shown the connection between the trade-off we obtained and the universal power-efficiency trade-off [44], $\Theta_0 \neq \Theta_1$ implies that, for heat engines with divergent physical quantities near the phase transition point, it is not possible to characterize the performance of the engine over the entire range of $\tilde{\eta}$ using a unified Θ. In other words, Θ is an implicit function of $\tilde{\eta}$ [45].

As a final remark, the presented results clearly demonstrate that the performance of our biochemical engine exceeds the universal power-efficiency trade-off obtained in the low-dissipation regime [11,12,14]. In this regime, the trade-off relation is determined by the typical irreversible entropy generation $S^{(\mathrm{ir})} = \Sigma/t$, where t is proportional to

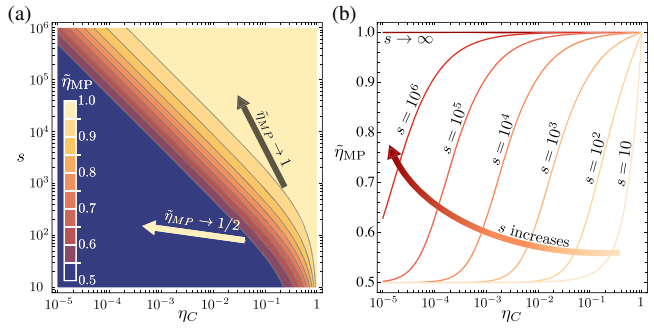


FIG. 3. (a) Rescaled EMP, $\tilde{\eta}_{\rm MP} \equiv \eta_{\rm MP}/\eta_C$, approaches 1 when $s \to \infty$ faster than $\eta_C \to 0$, breaking the $1/2$ universality. (b) $\tilde{\eta}_{\rm MP}$ as a function of η_C for different s.

cycle duration [9,46,47]. For noninteracting systems, both Σ and the reversible entropy change ΔS increase with the system size [12,13,47]. Consequently, the only way to reduce energy dissipation is to slow down the cycle operation, resulting in higher efficiency but lower output power. However, for many-body interacting systems, the relative value of Σ compared to ΔS can effectively be reduced by increasing the system size [21,25], enabling high-speed cycles that achieve Carnot efficiency when $S^{(\rm ir)}/\Delta S \to 0$. This observation is consistent with our results: in the geometric representation of the cycle [Figs. 2(a) and 2(d)], $\bar{W}_{\rm slow}$ and $\bar{W}_{\rm fast}$ respectively correspond to $S^{(\rm ir)}$ and ΔS. For a given cycle duration, $\bar{W}_{\rm slow}/\bar{W}_{\rm fast}$ decreases with s, eventually vanishing when $s \to \infty$.

Breaking the $1/2$ universality of EMP—For a heat engine operating in the linear-irreversible regime ($\Delta T/T_h \ll 1$), the leading-term coefficient of EMP with respect to η_C is $\alpha = 1/2$, irrespective of engine details [6,8,13,14]. However, this universality [29] relies on the validity of linear-irreversible thermodynamics and can be violated in the presence of divergent quantities [23,48]. Indeed, our minimal heat engine shows a violation of the $1/2$ universality when $s \to \infty$ due to the divergent slope of the equilibrium population curves, as demonstrated by Eq. (7). We notice that the order of taking $s \to \infty$ and $\eta_C \to 0$ significantly affects the result:

$$\lim_{\eta_C \to 0}\lim_{s \to \infty}\eta_{\rm MP} = \eta_C,$$
$$\lim_{s \to \infty}\lim_{\eta_C \to 0}\eta_{\rm MP} = \eta_C/2. \tag{14}$$

This implies that, in the parametric space (η_C, s), different limiting paths lead to different EMPs. By varying the limiting path, α transitions continuously from $1/2$ to 1, as shown by the color map of $\tilde{\eta}_{\rm MP} \equiv \eta_{\rm MP}/\eta_C$ in Fig. 3(a).

For finite-size working substances, one can always choose a small enough η_C to have the corresponding EMP approaching $\eta_C/2$ [Fig. 3(b)] [36]; thus the universality of $\lim_{\eta_C \to 0}\eta_{\rm MP} = \eta_C/2$ holds in the finite-size case. Consequently, the criterion to determine whether a heat engine is operating in the linear-irreversible regime should be $s\eta_C \ll 1$ instead of the conventional $\eta_C \ll 1$.

Conclusion—In this work, we propose a minimal model that highlights the absence of a general power-efficiency trade-off relation for heat engines with divergent quantities. The discrepancy between the EMP and Carnot efficiency is dictated by the system size, which is characterized by the number of microscopic states. Remarkably, Carnot efficiency at maximum power is attained in the thermodynamic limit with infinite system size. This observation aligns with recent findings on phase-transition-enhanced performance of heat engines [22,26].

Our minimal model also reveals the beneficial impact on heat engine performance of engineering microscopic states to form two coarse-grained states with distinct degeneracies, reinforcing earlier findings on the role of degeneracy and entropy in thermal systems [28,43,49–51]. These two states can be regarded as ordered and disordered states during a phase transition, achieved through collective effects in many-body interacting systems [22,25–27,43,52]. By focusing on the resulting energy-level structure rather than delving into the intricate interactions within many-body systems, our model succinctly and intuitively demonstrates how collective effects enhance the performance of heat engines. By introducing the idea of designing optimal internal structure for the engines' working substances, our approach will open up new avenues for optimizing heat engines, going beyond the conventional pursuit of optimal cycle control scheme [13,53–55].

Acknowledgments—The authors thank Simone Pigolotti for comments on a preliminary version of this manuscript. S. L. thanks the JSPS Strategic Fellowship for support under Grant No. GR22106. S. L. and P. D. L. R. thank the Swiss National Science Foundation for support under Grant No. 200020_178763. Y.-H. M. thanks the National Natural Science Foundation of China for support under Grant No. 12305037 and the Fundamental Research Funds for the Central Universities for support under Grant No. 2023NTST017. D. M. B. is funded by the program STARS@UNIPD with the project "ActiveInfo."

[1] H. B. Callen, *Thermodynamics and an Introduction to Thermostatistics* (John Wiley & Sons, New York, 1991).
[2] N. Shiraishi, K. Funo, and K. Saito, Speed limit for classical stochastic processes, Phys. Rev. Lett. **121**, 070601 (2018).
[3] P. Salamon and R. S. Berry, Thermodynamic length and dissipated availability, Phys. Rev. Lett. **51**, 1127 (1983).
[4] I. Novikov, The efficiency of atomic power stations (a review), J. Nucl. Energy (1954) **7**, 125 (1958).
[5] F. L. Curzon and B. Ahlborn, Efficiency of a Carnot engine at maximum power output, Am. J. Phys. **43**, 22 (1975).

[6] C. Van den Broeck, Thermodynamic efficiency at maximum power, Phys. Rev. Lett. **95**, 190602 (2005).

[7] T. Schmiedl and U. Seifert, Efficiency of molecular motors at maximum power, Europhys. Lett. **83**, 30005 (2008).

[8] Z. C. Tu, Efficiency at maximum power of Feynman's ratchet as a heat engine, J. Phys. A **41**, 312003 (2008).

[9] M. Esposito, R. Kawai, K. Lindenberg, and C. Van den Broeck, Efficiency at maximum power of low-dissipation Carnot engines, Phys. Rev. Lett. **105**, 150603 (2010).

[10] L. Chen and Z. Yan, The effect of heat-transfer law on performance of a two-heat-source endoreversible cycle, J. Chem. Phys. **90**, 3740 (1989).

[11] V. Holubec and A. Ryabov, Maximum efficiency of low-dissipation heat engines at arbitrary power, J. Stat. Mech. (2016) 073204.

[12] Y.-H. Ma, D. Xu, H. Dong, and C.-P. Sun, Universal constraint for efficiency and power of a low-dissipation heat engine, Phys. Rev. E **98**, 042112 (2018).

[13] H. Yuan, Y.-H. Ma, and C. P. Sun, Optimizing thermodynamic cycles with two finite-sized reservoirs, Phys. Rev. E **105**, L022101 (2022).

[14] R.-X. Zhai, F.-M. Cui, Y.-H. Ma, C. Sun, and H. Dong, Experimental test of power-efficiency trade-off in a finite-time Carnot cycle, Phys. Rev. E **107**, L042101 (2023).

[15] B. Andresen, Current trends in finite-time thermodynamics, Angew. Chem., Int. Ed. **50**, 2690 (2011).

[16] Z.-C. Tu, Abstract models for heat engines, Front. Phys. **16**, 1 (2021).

[17] *Finite-Time Thermodynamics*, edited by R. S. Berry, P. Salamon, and B. Andresen (MDPI—Multidisciplinary Digital Publishing Institute, Basel, Switzerland, 2022).

[18] N. Shiraishi, *An Introduction to Stochastic Thermodynamics: From Basic to Advanced*, Fundamental Theories of Physics Vol. 212 (Springer Nature, Singapore, 2023).

[19] M. Polettini and M. Esposito, Carnot efficiency at divergent power output, Europhys. Lett. **118**, 40003 (2017).

[20] J. S. Lee and H. Park, Carnot efficiency is reachable in an irreversible process, Sci. Rep. **7**, 10725 (2017).

[21] P. Abiuso and M. Perarnau-Llobet, Optimal cycles for low-dissipation heat engines, Phys. Rev. Lett. **124**, 110606 (2020).

[22] M. Campisi and R. Fazio, The power of a critical heat engine, Nat. Commun. **7**, 11895 (2016).

[23] U. Seifert, Efficiency of autonomous soft nanomachines at maximum power, Phys. Rev. Lett. **106**, 020601 (2011).

[24] A. E. Allahverdyan, K. V. Hovhannisyan, A. V. Melkikh, and S. G. Gevorkian, Carnot cycle at finite power: Attainability of maximal efficiency, Phys. Rev. Lett. **111**, 050601 (2013).

[25] A. Rolandi, P. Abiuso, and M. Perarnau-Llobet, Collective advantages in finite-time thermodynamics, Phys. Rev. Lett. **131**, 210401 (2023).

[26] H. Vroylandt, M. Esposito, and G. Verley, Collective effects enhancing power and efficiency, Europhys. Lett. **120**, 30009 (2018).

[27] F. S. Filho, G. A. L. Forão, D. M. Busiello, B. Cleuren, and C. E. Fiore, Powerful ordered collective heat engines, Phys. Rev. Res. **5**, 043067 (2023).

[28] H. Tajima and K. Funo, Superconducting-like Heat current: Effective cancellation of current-dissipation trade-off by quantum coherence, Phys. Rev. Lett. **127**, 190604 (2021).

[29] Z. C. Tu, Recent advance on the efficiency at maximum power of heat engines, Chin. Phys. B **21**, 020513 (2012).

[30] M. Grelier, D. A. Sivak, and J. Ehrich, Unlocking the potential of information flow: Maximizing free-energy transduction in a model of an autonomous rotary molecular motor, Phys. Rev. E **109**, 034115 (2024).

[31] C. Maffi, M. Baiesi, L. Casetti, F. Piazza, and P. De Los Rios, First-order coil-globule transition driven by vibrational entropy, Nat. Commun. **3**, 1065 (2012).

[32] S. Liang, D. M. Busiello, and P. D. L. Rios, Emergent thermophoretic behavior in chemical reaction systems, New J. Phys. **24**, 123006 (2022).

[33] A. V. Dass, T. Georgelin, F. Westall, F. Foucher, P. De Los Rios, D. M. Busiello, S. Liang, and F. Piazza, Equilibrium and non-equilibrium furanose selection in the ribose isomerisation network, Nat. Commun. **12**, 2749 (2021).

[34] C. Maes, Local detailed balance, SciPost Phys. Lect. Notes 32 (2021).

[35] L. Peliti and S. Pigolotti, *Stochastic Thermodynamics: An Introduction* (Princeton University Press, Princeton, NJ, 2021).

[36] See Supplemental Material at http://link.aps.org/supplemental/10.1103/PhysRevLett.134.027101 for analytical derivations and mathematical details of the stationary state in Sec. I, detailed discussion on the Otto cycle in Sec. II, power-efficiency trade-off in Sec. III, and the limit of EMP in Sec. IV.

[37] M. Esposito, Stochastic thermodynamics under coarse graining, Phys. Rev. E **85**, 041125 (2012).

[38] U. Seifert, Stochastic thermodynamics of single enzymes and molecular motors, Eur. Phys. J. E **34**, 26 (2011).

[39] At fixed temperatures and s, we numerically optimize power with respect to ϵ_h and ϵ_c to find the efficiency at maximum power. For the power-efficiency trade-off, we substitute $\epsilon_c = \epsilon_h(1 - \eta_C\tilde{\eta})$ and optimize power over ϵ_h under different $\tilde{\eta}$.

[40] P. Abiuso, P. A. Erdman, M. Ronen, F. Noé, G. Haack, and M. Perarnau-Llobet, Optimal thermometers with spin networks, Quantum Sci. Technol. **9**, 035008 (2024).

[41] R. Kawai, J. M. R. Parrondo, and C. V. den Broeck, Dissipation: The phase-space perspective, Phys. Rev. Lett. **98**, 080602 (2007).

[42] J. M. R. Parrondo, J. M. Horowitz, and T. Sagawa, Thermodynamics of information, Nat. Phys. **11**, 131 (2015).

[43] Y.-H. Ma, S.-H. Su, and C.-P. Sun, Quantum thermodynamic cycle with quantum phase transition, Phys. Rev. E **96**, 022143 (2017).

[44] N. Shiraishi, K. Saito, and H. Tasaki, Universal trade-off relation between power and efficiency for heat engines, Phys. Rev. Lett. **117**, 190601 (2016).

[45] This finding leaves an open question: does a tight analytical trade-off between power and efficiency exist throughout the entire range of $\tilde{\eta}$? We have attempted to find it but have not been successful so far. The asymptotic expressions in Eq. (10) at both ends of $\tilde{\eta}$ can serve as a good approximation for the complete trade-off relation in the large-s regime.

[46] I. A. Martínez, É. Roldán, L. Dinis, D. Petrov, J. M. Parrondo, and R. A. Rica, Brownian Carnot engine, Nat. Phys. **12**, 67 (2016).

[47] Y.-H. Ma, R.-X. Zhai, J. Chen, C. Sun, and H. Dong, Experimental test of the $1/\tau$-scaling entropy generation in finite-time thermodynamics, Phys. Rev. Lett. **125**, 210601 (2020).

[48] S. H. Lee, J. Um, and H. Park, Nonuniversality of heat-engine efficiency at maximum power, Phys. Rev. E **98**, 052137 (2018).

[49] N. Golubeva, A. Imparato, and M. Esposito, Entropy-generated power and its efficiency, Phys. Rev. E **88**, 042115 (2013).

[50] M. Esposito, K. Lindenberg, and C. V. den Broeck, Extracting chemical energy by growing disorder: Efficiency at maximum power, J. Stat. Mech. (2010) P01008.

[51] L. A. Correa, M. Mehboudi, G. Adesso, and A. Sanpera, Individual quantum probes for optimal thermometry, Phys. Rev. Lett. **114**, 220405 (2015).

[52] T. Herpich, J. Thingna, and M. Esposito, Collective power: Minimal model for thermodynamics of nonequilibrium phase transitions, Phys. Rev. X **8**, 031056 (2018).

[53] Y.-H. Ma, D. Xu, H. Dong, and C.-P. Sun, Optimal operating protocol to achieve efficiency at maximum power of heat engines, Phys. Rev. E **98**, 022133 (2018).

[54] A. G. Frim and M. R. DeWeese, Geometric bound on the efficiency of irreversible thermodynamic cycles, Phys. Rev. Lett. **128**, 230601 (2022).

[55] Y. Chen, J.-F. Chen, Z. Fei, and H. Quan, Microscopic theory of the Curzon-Ahlborn heat engine based on a Brownian particle, Phys. Rev. E **106**, 024105 (2022).